MECSOL 2022 - Proceedings of the 8th International Symposium on Solid Mechanics
M.L. Bittencourt, J. Labaki, L.C.M. Vieira Jr. and E. Mesquita (Editors), Campinas SP, Brazil, October 17th to 19th, 2022

Non-conforming Mesh Dynamical Substructuring: Case Study of a Tuned Mass Damper for a CubeSat

Guilherme Sobral de Albuquerque[1], Flávio Yukio Watanabe[1]

[1] Universidade Federal de São Carlos, Rod. Washington Luiz, s/n - Monjolinho, São Carlos - SP, 13565-905

Abstract. As a means of enabling the study of coupled structures from their subparts, Dynamic Substructuring is a technique, which has played a significant role in structural dynamics, and has been developed in order to better combine analytical and experimental models. This work presents a case study of a Tuned Mass Damper design for a pre-existing model of a CubeSat using two different approaches: Making a new system with two bodies, meshing the structure and getting the modal analysis via Finite Element Analysis; and reusing the model of the satellite, making a new one for the damper alone and assembling both via Dynamic Substructuring. While the former approach results in a new model with no loss of accuracy, the latter enables a faster development – reducing time both by facilitating parallel design for each of the substructures, and by reducing the computational time on the iterations of multiple simpler parts instead of a complex one –, as well as a better understanding of the individual parts of the system, such as the main modes of vibration and respective frequencies, which in this case could be used as a starting point for the fine-tuning of the damper design, all while maintaining a high-fidelity model of the full system. The model was analyzed regarding its response in the frequency range of interest, with respect to the deformations of the most fragile areas in the structure. The analysis of the assembled system was then compared to the full-model simulation (with conformed contact meshing) in order to validate the model, as well as the method. The frequency response functions were similar, and the relative error for the resonance frequencies was less than 0.2%, indicating the success of the method in keeping the model's fidelity.
Keywords: Dynamic Vibration Absorber, Miniaturized Satellite, Finite Element Method, Modal Analysis, Dynamic Substructuring.

INTRODUCTION

Numeric methods and advancements on computational technologies allow engineers to analyze complex structures with high fidelity still on the development stage (Akcay Perdahcioglu et al., 2013). One of the most widely used tools to study structures is the Finite Element Analysis (FEA), but while the method gives a reliable result, analyzing a complex structure may lead to models which are computationally hard to deal with.

Since, in general, the low frequency vibration modes are the main interest, the amount necessary of degrees of freedom to analyze the model can be greatly reduced compared to the ones necessary to create a high fidelity mesh, such that complex systems are usually analyzed in a reduced form (Hatch, 2001).

Besides reducing complex models, it's also possible to divide the structure in smaller parts, generate their individual models and couple them via Dynamic Substructuring (DS), a technique introduced by Craig and Bampton (1968). In addition to saving costs and development time, the analytical capability to foresee a structure's response knowing only its parts can be necessary in some applications. For instance, spacial components need to be well characterized and tested before being entirely assembled (Allen et al., 2020), making DS a powerful tool to analyze such systems.

In General, mechanical simulation software programs use Substructuring to couple different bodies, generating a conforming mesh in shared interfaces. However, when the models are made separately, it's not usually trivial to couple the interface region.

Many methods can be used in order to merge structures with different meshes. One can create filter matrices, effectively making a weak coupling, where only a linear combination of the contact nodes are compatible, such as the mean movement, as described in Bernardi et al. (1994). Another option is to generate a common mesh between the bodies, such that there's a conforming region to help to couple (Akcay Perdahcioglu et al., 2013). This work aims to study the effects of applying the coupling only on a geometrically-chosen subset of contact region mesh nodes. In order to do so, a case study of a Tuned Mass Damper design for a pre-existing model of a CubeSat will be used.

DYNAMIC SUBSTRUCTURING

A general linear system with N degrees of freedom has an equation of motion according to Eq. (1) (Fu and He, 2001).

$$\mathbf{M}\ddot{x} + \mathbf{C}\dot{x} + \mathbf{K}x = f, \tag{1}$$

where $\mathbf{M}$, $\mathbf{C}$ and $\mathbf{K}$ are the $N \times N$ mass, damping and stiffness matrices, respectively. The terms x, $\dot{x}$ and $\ddot{x}$ are the $N \times 1$ displacement, velocity and acceleration vectors, and f is the external forces vector.

In order to couple different systems via Dynamic Substructuring, the distinct parts' connection is made from two interface conditions: coordinate *compatibility* — i.e, all substructure's nodes on the interface must have the same displacement —, and interface forces *equilibrium* — which must have same magnitude and opposite signs (van der Seijs, 2016).

Considering two bodies, A and B, whose internal Degrees of Freedom (DOFs) are, respectively, u_1^{A} and u_3^{B} are connected in the interface which is composed by the u_2^{A} and u_2^{B} DOFs, and whose contact forces are given by g_2^{A} and g_2^{B}, as is shown in Fig. 1.

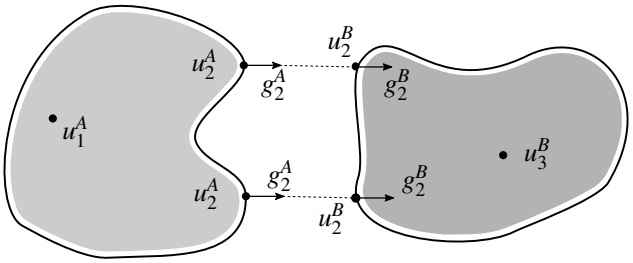

Figure 1 – Coupling between structures A and B.

Then, the compatibility and equilibrium conditions can be written, respectively as

$$\begin{cases} u_2^{\mathrm{A}} = u_2^{\mathrm{B}} \\ g_2^{\mathrm{A}} + g_2^{\mathrm{B}} = 0. \end{cases} \tag{2}$$

By defining the following vectors

$$u \triangleq \begin{bmatrix} u_1^{\mathrm{A}} \\ u_2^{\mathrm{A}} \\ u_2^{\mathrm{B}} \\ u_3^{\mathrm{B}} \end{bmatrix}, \quad f \triangleq \begin{bmatrix} f_1^{\mathrm{A}} \\ f_2^{\mathrm{A}} \\ f_2^{\mathrm{B}} \\ f_3^{\mathrm{B}} \end{bmatrix}, \quad g \triangleq \begin{bmatrix} 0 \\ g_2^{\mathrm{A}} \\ g_2^{\mathrm{B}} \\ 0 \end{bmatrix}, \tag{3}$$

being f the external forces vector, the equilibrium condition can be expressed by choosing a set of generalized coordinates q. The set contains the unique coordinates that are left by coupling the structure — that is, each pair of DOFs on the interface is described by only one generalized coordinate, which implies the compatibility condition is satisfied by default. Expressing u in terms of q results in

$$u = \mathbf{L}q \implies \mathbf{L} \triangleq \begin{bmatrix} \mathbf{I} & \mathbf{0} & \mathbf{0} \\ \mathbf{0} & \mathbf{I} & \mathbf{0} \\ \mathbf{0} & \mathbf{I} & \mathbf{0} \\ \mathbf{0} & \mathbf{0} & \mathbf{I} \end{bmatrix}, \tag{4}$$

where $\mathbf{L}$ is called the *boolean localization matrix*.

The equilibrium condition can also be written using $\mathbf{L}$:

$$\mathbf{L}^{\mathrm{T}} g = 0 \implies \begin{cases} g_1^{\mathrm{A}} = 0 \\ g_2^{\mathrm{A}} + g_2^{\mathrm{B}} = 0 \\ g_3^{\mathrm{B}} = 0. \end{cases} \tag{5}$$

Considering a system in physical domain, the equations of motion for a given substructure (s) is

$$\mathbf{M}^{(s)}\ddot{u}^{(s)} + \mathbf{C}^{(s)}\dot{u}^{(s)} + \mathbf{K}^{(s)}u^{(s)} = f^{(s)} + g^{(s)}. \tag{6}$$

By defining the system matrices as the block diagonal for all substructures, that is $\mathbf{M} = \text{diag}(\mathbf{M}^{(1)}, \ldots, \mathbf{M}^{(n)})$ and analogously for $\mathbf{C}$ and $\mathbf{K}$, the *uncoupled* system of equations for the whole structure is

$$\mathbf{M}\ddot{u} + \mathbf{C}\dot{u} + \mathbf{K}u = f + g \tag{7}$$

Using a global coordinate system q, such that $u = \mathbf{L}q$ (compatibility) and setting $\mathbf{L}^{\mathrm{T}}g = 0$ (equilibrium), the system becomes

$$\begin{cases} \mathbf{M}\mathbf{L}\ddot{q} + \mathbf{C}\mathbf{L}\dot{q} + \mathbf{K}\mathbf{L}q = f + g \\ \mathbf{L}^{\mathrm{T}}g = 0. \end{cases} \tag{8}$$

By premultiplying Eq. (8) by $\mathbf{L}^{\mathrm{T}}$, the unknown forces can be removed:

$$\mathbf{L}^{\mathrm{T}}\left(\mathbf{M}\mathbf{L}\ddot{q} + \mathbf{C}\mathbf{L}\dot{q} + \mathbf{K}\mathbf{L}q = \mathbf{L}^{\mathrm{T}}f + 0\right) \tag{9}$$

$$\implies \tilde{\mathbf{M}}\ddot{q} + \tilde{\mathbf{C}}\dot{q} + \tilde{\mathbf{K}}q = \tilde{f}, \quad \text{with} \quad \begin{cases} \tilde{\mathbf{M}} \triangleq \mathbf{L}^{\mathrm{T}}\mathbf{M}\mathbf{L} \\ \tilde{\mathbf{C}} \triangleq \mathbf{L}^{\mathrm{T}}\mathbf{C}\mathbf{L} \\ \tilde{\mathbf{K}} \triangleq \mathbf{L}^{\mathrm{T}}\mathbf{K}\mathbf{L} \\ \tilde{f} \triangleq \mathbf{L}^{\mathrm{T}}f \end{cases}. \tag{10}$$

This way, Eq. (10) shows the equations of motion for the coupled system of equations. This method of using the unique coordinate system is called *Primal Assembly*.

NON-CONFORMING MESHING

Constructing the Boolean localization matrix $\mathbf{L}$ depends on the connected DOFs. For a three-dimensional mesh model with solid elements, each node usually carries 3 (translational) DOFs, so that finding which nodes are connected is enough.

However, for models in which the interface nodes do not have a one-to-one correspondence, there is another problem to be considered. Allen et al. (2020) discusses a few techniques for dealing with that, such as using a filter matrix for the connection matrices, effectively making a weak coupling, where only the means of the nodes movements are coupled.

This work will analyze the quality of an analysis in which nodes are coupled by geometric proximity, on a subset of the interface nodes, as is shown in Fig. 2.

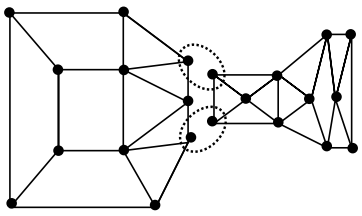

Figure 2 – Schematic of two structures with non-conforming meshes coupled by node proximity.

CASE STUDY

Problem

As a case study, a problem that arose during the development of a CubeSat nanosatellite by the Zenith Aerospace group from the São Carlos School of Engineering on the University of São Paulo (EESC/USP) will be analyzed.

A Modal Analysis was made on Ansys Workbench 2021 simulating launching conditions for the structure. The first mode of vibration happens below the expected launching excitation bandwidth. This mode happens on the satellite's walls (on which circuit boards are expected to be mounted), with displacement normal to its surface, as is shown in Fig. 3.

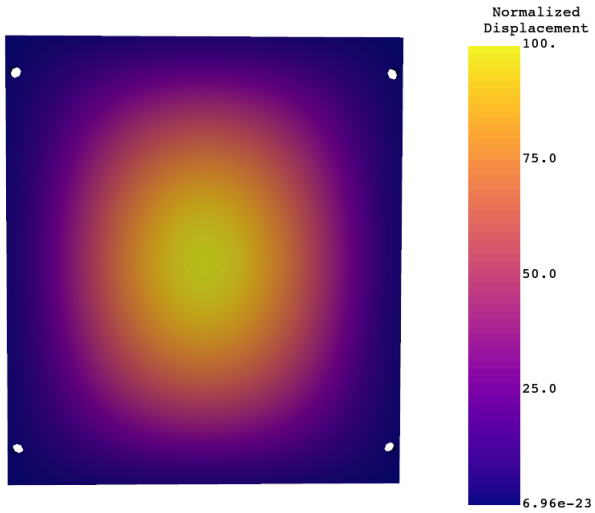

Figure 3 – Normalized displacement for the first mode of vibration of the CubeSat's wall.

This mode of vibration happens at 1990 Hz, within the expected bandwidth designated by GSFC (2021), as shows the Acceleration Spectral Density profile on Table 1.

Table 1 – Qualification and acceptance values for external excitation in random vibration tests for CubeSat deployment. Source: GSFC (2021).

	Qualification	Acceptance
Frequency (Hz)	ASD (g^2/Hz)	ASD (g^2/Hz)
20	0.026	0.013
20 – 80	+6 dB/oct	+6 dB/oct
80 – 500	0.16	0.08
500 – 2000	-6 dB/oct	-6 dB/oct
2000	0.026	0.013
Total	14.1 Grms	10.0 Grms

Since the system's stiffness was already high, increasing it can be difficult, so a possibility is to couple it to a Tuned Mass Damper (TMD).

Tuned Mass Damper

A tuned mass damper is a mechanical device used to reduce unwanted vibrations (Rao, 2017). It consists of a mass and stiffness added to the original structure that needs to be sheltered from vibration. Idealizing the main structure as a one-dimensional system of mass m_1 and stiffness to the ground k_1, by coupling an auxiliary mass m_2 with stiffness k_2 and damping c_2, the result system is depicted in Fig. 4.

The stationary amplitude for the equation of motion of the system under external force of type $F_0 \sin \omega t$ is given by

$$X_1 = \frac{F_0(k_2 - m_2\omega^2 + \mathrm{j}c_2\omega)}{[(k_1 - m_1\omega^2)(k_2 - m_2\omega^2) - m_2k_2\omega^2] + \mathrm{j}\omega c_2(k_1 - m_1\omega^2 - m_2\omega^2)}. \tag{11}$$

The general response of the system can be seen on Fig. 5.

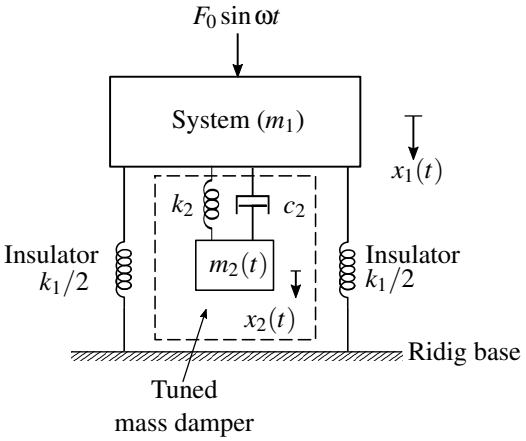

Figure 4 – Tuned mass damper. Source: Rao (2017).

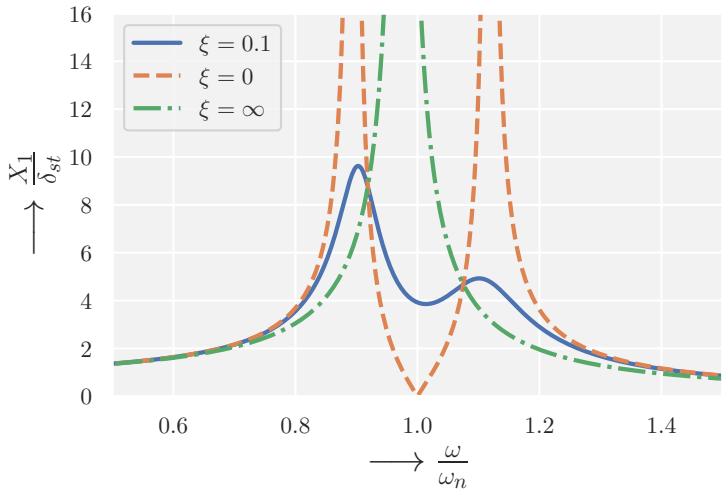

Figure 5 – System response with TMD for different damping ratios ξ.

Here, $\delta_{st} = F_0/k_1$. Parameters of $k_1/m_1 = k_2/m_2 = \omega_n^2$ and $m_2 = 0.05m_1$. Varying the TMD'S damping ratio $\xi = c_2/2\sqrt{k_2 m_2}$ gives different behaviors for the system. The result of $\xi = 0$ is the response of an undamped vibration absorber; for $\xi \to \infty$, the system behaves as the original system with no absorber, but with a slightly higher mass; and for $\xi = 0.1$ the typical desired system with a TMD is seen.

TMD design

The TMD was designed in a cylindrical shape, whose coupling is made via 3 points with the CubeSat's wall. Its shape was chosen as having a fine membrane with a concentrated mass on its center, fine-tuned such that its natural frequency (with the 3 points of contact fixed) were close to the CubeSat's first mode of vibration. A schematic of its side view can be seen in Fig. 6.

The modeled Computer-Aided Design (CAD) of the TMD casing and membrane be seen in Figure 7. The 3 discrete contact points can be seen on the casing, while the mass concentration can be seen on the membrane.

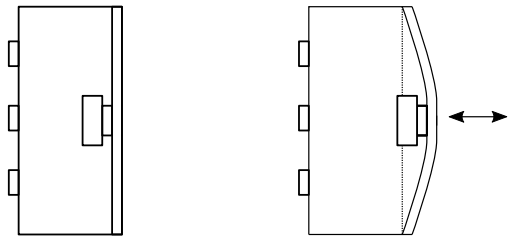

Figure 6 – Schematic of the designed TMD's interior.

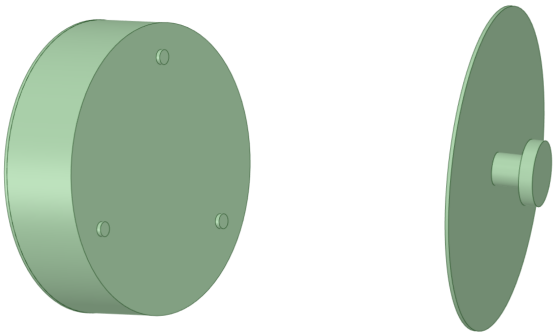

Figure 7 – TMD's casing (left) and membrane (right) with concentrated mass CAD design.

The material chosen for the design as lead, for its high density, so that the TMD does not occupy too much space of the already restrained CubeSat. The cylinders' size and membrane width were chosen such that the effective mass m_2, stiffness k_2, and damping coefficient c_2 (as described in Figure 4) were, respectively, 20 mg, 3.4 N/mm and 4.0×10^{-3} Ns/m.

The natural frequency of the system's first mode of vibration was 2060.8 Hz, simulated also via Ansys Workbench 2021 Modal Analysis. Its free-free model was then exported in order to couple it to the CubeSat's via DS, after choosing its connected nodes.

Geometric mesh connection

In order to realize the primal assembly of the substructures (CubeSat and TMD), their mass and stiffness matrices are needed ($\mathbf{M}^{\mathrm{A}}$, $\mathbf{K}^{\mathrm{A}}$, $\mathbf{M}^{\mathrm{B}}$ and $\mathbf{K}^{\mathrm{B}}$), but also the localization matrix $\mathbf{L}$, which requires knowledge about which DOFs to connect.

The method used was to choose geometrically the meshes nodes, via proximity, and then couple the corresponding DOFs. The meshes can be seen in Fig. 8. The meshes were exported from Ansys and handled in python using the `pyansys` (Kaszynski, 2020).

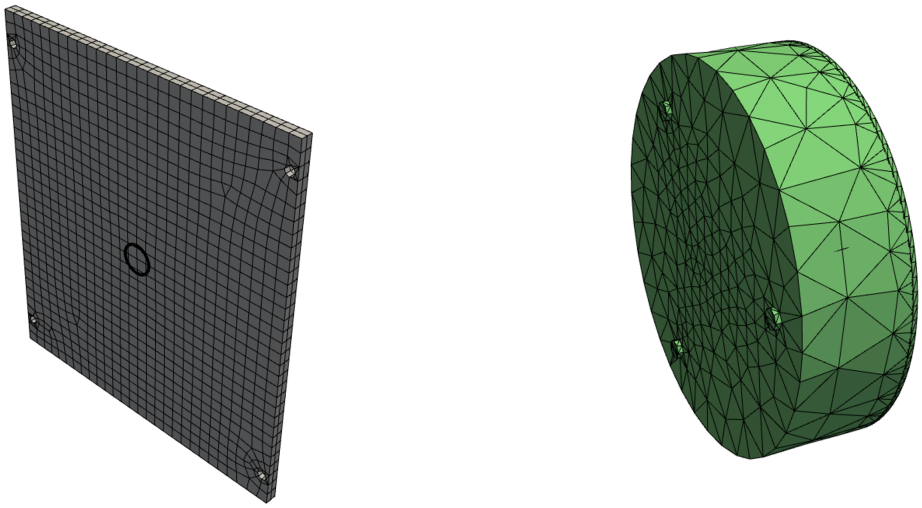

Figure 8 – Meshes exported from Ansys. CubeSat's wall on the left and TMD on the right.

Joining the meshes on the same space, the three contact surfaces can be used in order to find the correct translations and rotations that couple the structures. After processing said manipulations, the interface nodes superposed can be seen on Fig. 9.

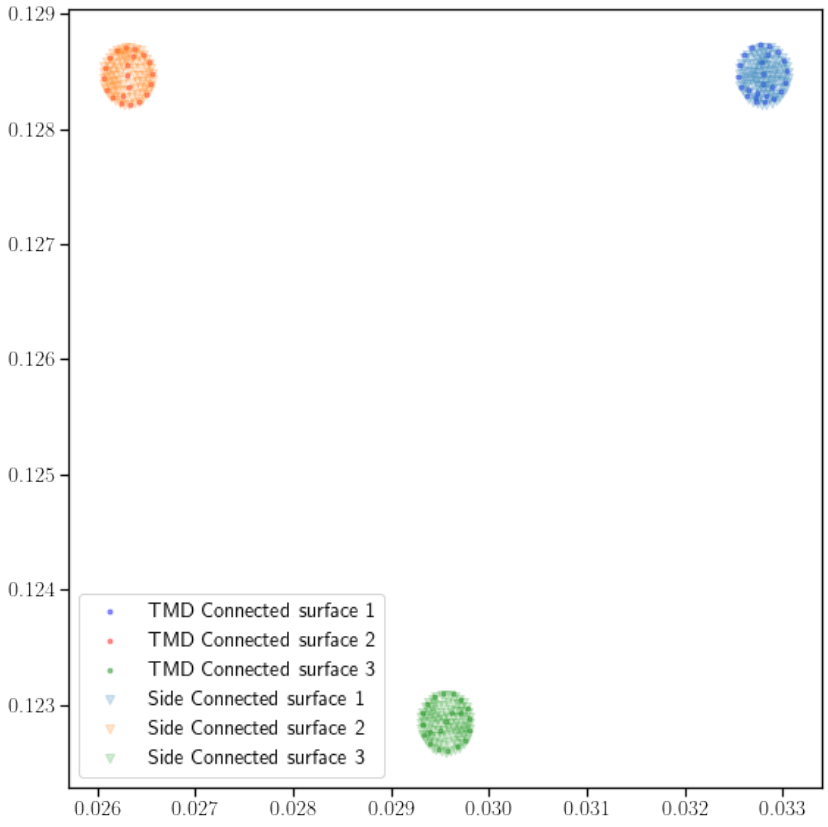

Figure 9 – Superposed interface nodes for both structures.

It can be seen that the meshes are non-confirming, since the wall's mesh has a higher node density, and not all of

TMD's nodes have a corresponding node on the wall's mesh. For simplicity, only the external nodes were used for the coupling Fig. 10.

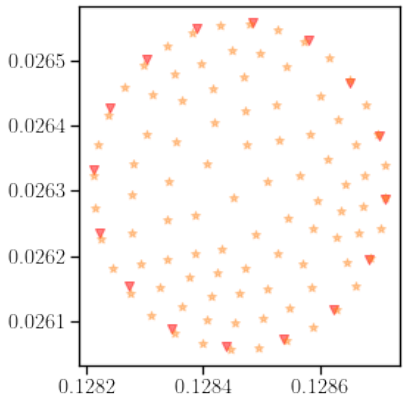

Figure 10 – External TMD points chosen for assembly.

Then, the closest node from the wall's mesh was chosen, so that the boolean matrix $\mathbf{L}$ could be created and the primal assembly of the structures could be made (see Figure 11).

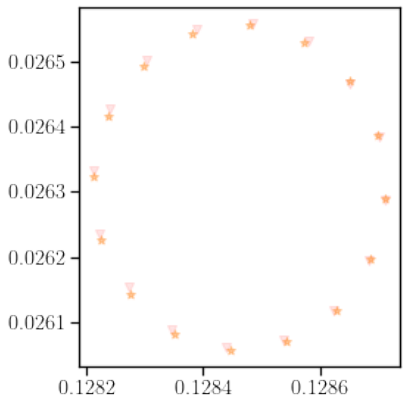

Figure 11 – Corresponding nodes from wall.

From this coupling, the results discussed previously can be applied to find the assembled structure's response.

RESULTS

The system's response before and after the coupling can be seen in Fig. 12.

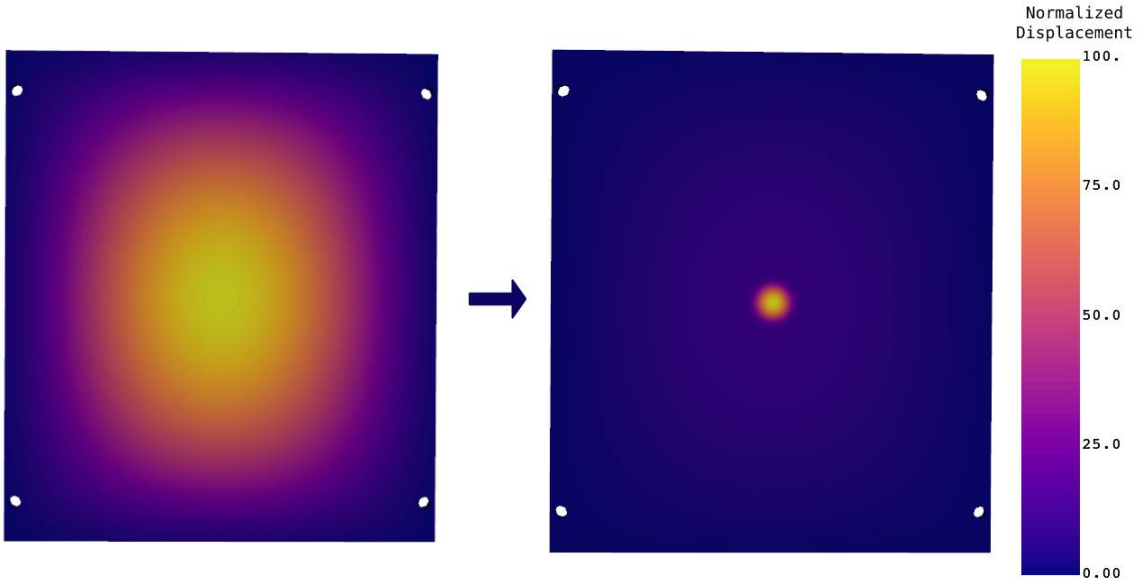

Figure 12 – Normalized displacement for the first mode of vibration of the CubeSat's wall before (left) and after coupling (right) the TMD. The normalization happens individually for each system.

The displacement profiles show that the device is causing the wanted effect, that is, the movement is concentrated on the TMD's membrane, while the CubeSat's wall movement is attenuated. A further harmonic analysis of both systems being measured on the center region gives that the peak displacement of the Frequency Response Function (FRF) is 17 times smaller with the device.

In order to assess the fidelity of the primal assembly, a full model was made on Ansys with conforming meshing. The FRFs comparing the responses (and also with the model without the TMD) can be seen on Fig. 13.

The x direction is normal to the wall's surface, and the y direction is aligned with gravity.

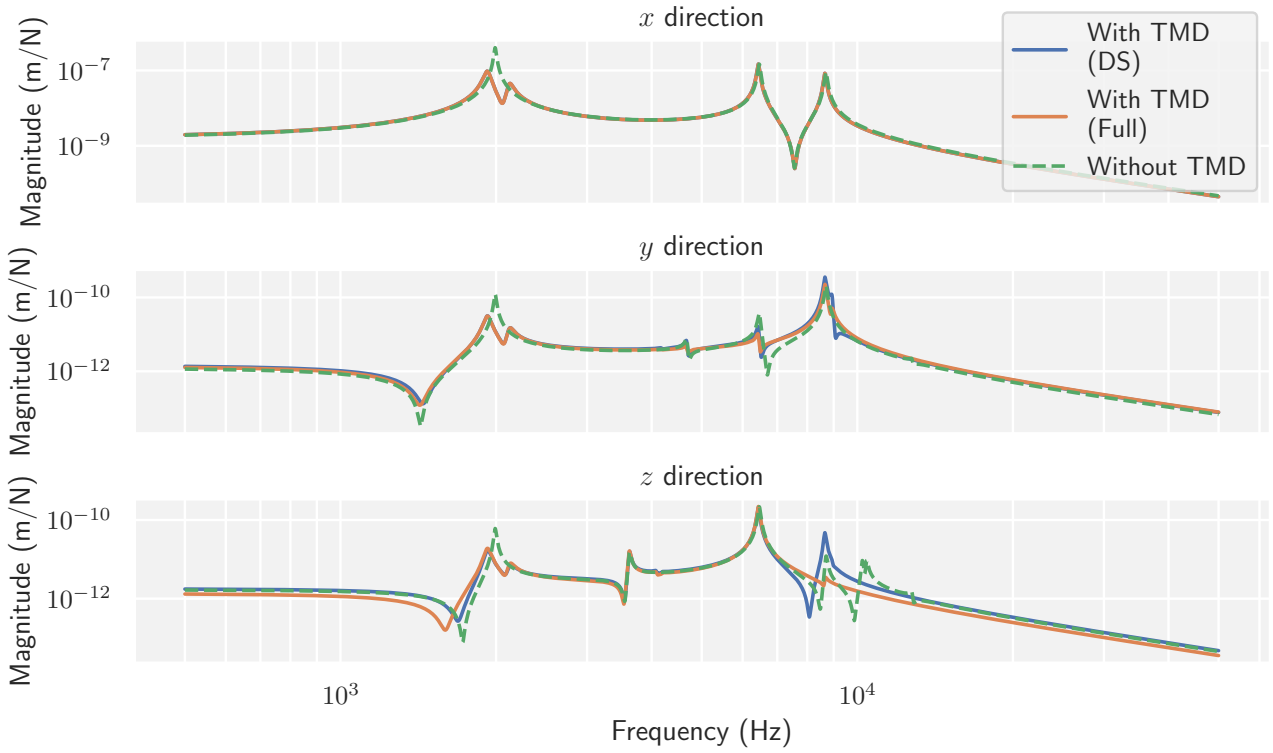

Figure 13 – Comparison between FRFs magnitudes for the structure with and without TMD, and also for a full model made directly on Ansys.

The graph shows the expected behavior difference of coupling a TMD near 2000 Hz. The main peak was split into two smaller peaks, while the rest of the frequency region does not see much change.

It can be seen that the response is of much greater magnitude on the x direction. In this direction, the graphs of the assembled structures (either with conforming or non-conforming meshes) seem indistinguishable. On the other graphs it can be seen a difference of behavior near 9000 Hz, but its amplitude is considerably smaller than the x response. Also, at that high frequency, the FRF starts to decrease indefinitely, indicating that there may be too few elements per wavelength at that frequency, such that the response is not as precise in this region, even for the original model.

Besides that, on Table 2, the relative error in frequency between the first 10 modes of vibration can be seen, relating both methods.

Table 2 – Comparison between frequency values of the first 10 modes of vibration of the coupled structure for the two modes of assembly, with the respective errors.

Mode	Ansys [Hz]	DS [Hz]	Relative error
1	1924.00	1924.04	0.002%
2	2120.02	2119.17	−0.040%
3	3619.22	3621.04	0.050%
4	4087.48	4087.16	−0.008%
5	4183.71	4182.99	−0.017%
6	4675.87	4679.99	0.088%
7	6246.48	6245.97	−0.008%
8	6435.20	6433.78	−0.022%
9	8654.22	8652.29	−0.022%
10	8925.29	8939.26	0.156%

Table 2 shows that the lowest error is less than 0.2 % for the first 10 modes of vibration, which is well within the accuracy of the model itself, showing that the method is successful in keeping a high accuracy for a stiff contact region.

CONCLUSION

From the model of the CubeSat's wall coupled to the TMD device and its first mode of vibration, it could be seen that the displacements were focused on the damper, such that the CubeSat's amplitudes diminished considerably, which can also be seen by the Frequency Response Function of the system with and without the device. The viability of using the designed TMD on a future CubeSat launching, however, does not follow directly from these results. Since the model was simplified, a specific device would need to be designed for each possible satellite.

Comparing the model coupled via primal assembly on non-conforming meshes using only a subset of nodes with the full model with conforming mesh, it was possible to analyze the fidelity of the presented method. Even though the Frequency Response Function exhibited divergence in some parts, they happened in higher frequencies and in directions in which the displacement amplitude was orders of magnitude lower than the principal. Furthermore, the most significant values for the analysis — that is, the resonance frequencies — were all under 0.2 % up to 9000 Hz, where even the original model starts losing accuracy, proving the method a robust tool for a numeric analysis.

Thus, this method proves useful for enabling the development of complex dynamic models in parallel, fine-tuning structures separately and coupling *a posteriori*, as well as updating a complex model from the coupling of simpler structures, without the need to redo the whole model, possibly saving up a lot of development time.

REFERENCES

Akcay Perdahcioglu, D., Doreille, M., de Boer, A. and Ludwig, T., 2013, "Coupling of non-conforming meshes in a component mode synthesis method". International Journal for Numerical Methods in Engineering, 96(6), 390–404. https://doi.org/10.1002/nme.4575

Allen, M. S., Mayes, R. L. and Tiso, P., 2020, "Short Course on Experimental Dynamic Substructuring". https://substructure.engr.wisc.edu/substwiki/index.php?title=Tutorials

Bernardi, C., Maday, Y. and Patera, A. T., 1994, "A new nonconforming approach to domain decomposition: The mortar element method. Nonlinear partial differential equations and their applications". Collège de France Seminar, volume XI. Lectures presented at the weekly seminar on applied mathematics, 13–51.

Craig, R. R. and Bampton, M. C., 1968, "Coupling of substructures for dynamic analyses". AIAA Journal, 6(7), 1313–1319. https://doi.org/10.2514/3.4741

Fu, Z. F. and He, J., 2001, "Modal Analysis". Elsevier. https://doi.org/10.1016/b978-0-7506-5079-3.x5000-1

GSFC-STD-7000B, 2021, "General Environmental Verification Standard (GEVS) for GFSC flight programs and projects". U.S. National Aeronautics and Space Administration. https://standards.nasa.gov/standard/gsfc/gsfc-std-7000

Hatch, M. R., 2001, "Vibration Simulation Using MATLAB and ANSYS". Chapman & Hall/CRC. https://doi.org/10.1201/9781420035759

Kaszynski, A., 2020, "pyansys: Python Interface to MAPDL and Associated Binary and ASCII Files". https://doi.org/10.5281/zenodo.4009467

Rao, S. S., 2017, "Mechanical Vibrations Sixth Edition in SI Units". Access for. Pearson, 6, 1291.

van der Seijs, M., 2016, "Experimental Dynamic Substructuring Analysis and Design Strategies for Vehicle Development". https://doi.org/10.4233/uuid:28b31294-8d53-49eb-b108-284b63edf670

RESPONSIBILITY NOTICE

The author(s) is (are) the only party(ies) responsible for the printed material included in this paper.